Monthly Notices
of the
ROYAL ASTRONOMICAL SOCIETY

Mon. Not. R. Astron. Soc. **402,** 1758–1766 (2010) doi:10.1111/j.1365-2966.2009.15994.x

The orbital decay of embedded binary stars

Steven W. Stahler★

Astronomy Department, University of California, Berkeley, CA 94720, USA

Accepted 2009 November 5. Received 2009 October 30; in original form 2009 July 31

ABSTRACT

Young binaries within dense molecular clouds are subject to dynamical friction from ambient gas. Consequently, their orbits decay, with both the separation and period decreasing in time. A simple analytic expression is derived for this braking torque. The derivation utilizes the fact that each binary acts as a quadrupolar source of acoustic waves. The acoustic disturbance has the morphology of a two-armed spiral and carries off angular momentum. From the expression for the braking torque, the binary orbital evolution is also determined analytically. This type of merger may help in explaining the origin of high-mass stars. If infrared dark clouds, with peak densities up to 10^7 cm^{-3}, contain low-mass binaries, those with separations less than 100 au merge within about 10^5 years. During the last few thousand years of the process, the rate of mechanical energy deposition in the gas exceeds the stars' radiative luminosity. Successive mergers may lead to the massive star formation believed to occur in these clouds.

Key words: binaries: general – stars: early-type – stars: formation – ISM: clouds.

1 INTRODUCTION

The youngest binaries are still embedded in molecular cloud gas. During this phase, the orbiting components experience dynamical friction with the surrounding medium. The braking torque causes the stars to spiral inwards, so that their separation and period diminish with time. Such orbital decay may be significant in the very densest molecular clumps. In particular, infrared dark clouds, currently believed to be the birthsites of massive stars, have peak number densities as high as 10^7 cm^{-3} (Rathborne, Jackson & Simon 2006; Beuther et al. 2007). This impressive figure matches that in hot molecular cores, already known to contain luminous, high-mass objects (Kurtz et al. 2000). Binary mergers could be occurring in these environments and could play a role in forming the massive stars.

There is still no direct evidence that either infrared dark clouds or hot molecular cores contain low-mass stars. However, observations show that, with few exceptions, massive stars originate in populous clusters (de Wit et al. 2005). Indeed, one account of high-mass star formation is that it proceeds through the coalescence of lower mass cluster members (Bonnell, Bate & Zinnecker 1998; Stahler, Palla & Ho 2000). At even the highest observed cluster densities, collisions between stars, either bare or with extended discs, occur at too low a frequency. However, the presence of dense, background gas should enhance the capture rate (Bally & Zinnecker 2005). Specifically, the braking torque from dynamical friction might not only shrink initially wide binaries, but cause the component stars to merge. An accelerating succession of such mergers could then build up massive stars.

To assess this possibility, the present study calculates the torque on a binary embedded within an extensive gas cloud. Although the torque is created by dynamical friction, the usual analysis of that effect is difficult to apply in this context. Following Dokuchaev (1964), theorists have determined the frictional drag on a single mass travelling through ambient gas in a straight line (see also Ruderman & Spiegel 1971; Rephaeli & Salpeter 1980; Ostriker 1999). Just as in the stellar dynamical case (Chandrasekhar 1942), the moving mass draws external matter into a trailing wake. It is the gravitational tug from this wake that provides the effective drag. The same essential mechanism is at work in the case of a binary. However, the trajectories of both perturbing masses are now closed orbits. Further complicating the analysis is the fact that each star draws in matter from the wake of its companion. Naive application of the standard dynamical friction formulae would grossly misestimate the torque.

The new approach introduced here concentrates on the fact that the binary as a whole must shed angular momentum to the external medium. The actual mechanism is that the orbiting stars create an oscillating gravitational potential that torques nearby gas. This fluctuating torque generates outgoing acoustic waves, which transport angular momentum. By calculating the total angular momentum efflux from the binary, the braking torque may be obtained without considering the complex star–gas interaction close to the stars themselves.

Section 2 below formulates the problem mathematically and derives the governing wave equation. The quadrupolar driving potential created by the rotating stars is established in Section 3, while Section 4 discusses the physical character of the generated waves.

★E-mail: Sstahler@astro.berkeley.edu

Section 5 presents the central result of this investigation. Here the angular momentum transported by the spiral wave is obtained, and thereby the torque (see equation 39). It is also shown that the wave carries off all the mechanical energy released by the shrinking binary. The resulting temporal evolution of the system is considered in Section 6, along with the efficacy of braking in infrared dark clouds. Finally, Section 7 compares the results obtained here with the traditional analysis and discusses future extensions of this study.

2 FORMULATION OF THE PROBLEM

2.1 Length-scales

We wish to treat the binary as a perturbing mass embedded in otherwise static, uniform gas. If the binary itself is recently formed, then gas surrounding it would not be perfectly quiescent. Hence, our assumed background is a highly idealized representation of a real cloud, or at least that portion of a cloud in which we can accurately follow the propagation of acoustic waves from the stars. One obvious stipulation is that this region cannot be so close to the binary that cloud gas is infalling onto the stars. This requirement sets an inner radius of validity for the analysis, which we take to be the sonic point in the Bondi accretion problem:

$$r_{\rm in} \equiv G\,M_{\rm tot}/2\,c_{\rm s}^2 \tag{1a}$$

$$= 100\,{\rm au}\left(\frac{M_{\rm tot}}{1{\rm M}_\odot}\right)\left(\frac{c_{\rm s}}{2\ {\rm km\ s^{-1}}}\right)^{-2}. \tag{1b}$$

Here, $M_{\rm tot}$ is the total binary mass and $c_{\rm s}$ is the sound speed of the surrounding gas, assumed to be isothermal. In the numerical evaluation of $r_{\rm in}$, we have used for $c_{\rm s}$ the typical observed velocity dispersion of infrared dark clouds (Sridharan et al. 2005).[1] Inside $r_{\rm in}$, where the binary itself may reside, gas falls freely onto the central stars.

If the binary separation, to be denoted as $a_{\rm tot}$, exceeds $r_{\rm in}$, then each orbiting star is surrounded by its own zone of infall. In that case, $a_{\rm tot}$ becomes the appropriate inner boundary. This comparison of $a_{\rm tot}$ relative to $r_{\rm in}$ effectively distinguishes two cases: 'hard' binaries, in which the relative speed of the component stars is supersonic with respect to the gas ($a_{\rm tot} < r_{\rm in}$), and 'soft' binaries, for which this speed is subsonic ($a_{\rm tot} > r_{\rm in}$). We shall concentrate on the first case, since it yields, as we shall see in Section 4, a simplified form of the acoustic disturbance.

We also require that our propagation region is not so spatially extended that the dominant gravitational force is from interior gas rather than the stars. Thus, we are confined within another radius $r_{\rm gas}$, where the mass of background gas rivals that of the stars. For an H_2 number density of $10^7\ {\rm cm^{-3}}$, representing the most compact regions of infrared dark clouds, we find that $1\,{\rm M}_\odot$ is contained in $r_{\rm gas} = 1600$ au. Beyond even this point, the theory indicates, and observations confirm (e.g. Butler & Tan 2009), that the mass density ρ falls off in response to the self-gravity of the cloud as a whole. This outermost radius is the Jeans length $\lambda_{\rm J}$, where

$$\lambda_{\rm J} \equiv \frac{c_{\rm s}}{\sqrt{G\,\rho}} \tag{2a}$$

$$= 9\times10^3\,{\rm au}\left(\frac{n}{10^7\ {\rm cm^{-3}}}\right)^{-1/2}\left(\frac{c_{\rm s}}{2\ {\rm km\ s^{-1}}}\right). \tag{2b}$$

Our wave analysis is thus valid within a somewhat restricted, but well-defined, dynamic range.

By the same token, we *cannot* model, using this method, binaries embedded within the dense cores characterizing low-mass star formation environments (see Haisch et al. (2004) for observations of candidate stellar pairs). Here, the entire cloud mass is comparable to the stellar $M_{\rm tot}$, and $a_{\rm tot} < r_{\rm in} \sim r_{\rm gas} \sim \lambda_{\rm J}$. Physically, the dynamics inside such a dense core are dominated by infall onto the binary, unless the cloud is stabilized by tension in its internal magnetic field. Acoustic waves may propagate outside the cloud, but their source would be both the stars and the dense core gas.

2.2 Perturbation analysis

We now introduce our central object, the binary. Let the component stars have masses M_1 and M_2, whose values are in the ratio q, where $q < 1$. We assume, for simplicity, that the two are on circular orbits about their mutual centre of mass, with radii a_1 and a_2. For a given $M_{\rm tot}$, q and $a_{\rm tot} \equiv a_1 + a_2$, the fixed separation between the stars, we want to ascertain the perturbing effect of the binary on the surrounding cloud, taken to have a background density of ρ_0.

In the linear approximation valid for small disturbances, momentum conservation reads

$$\frac{\partial \boldsymbol{u}_1}{\partial t} = -\frac{c_{\rm s}^2}{\rho_0}\,\nabla\rho_1 - \nabla\Phi_1^*. \tag{3}$$

Here, we have denoted the small induced velocity by $\boldsymbol{u}_1$ and have used the same subscript for perturbations in the density and potential. The superscript on Φ_1^* emphasizes that this perturbation is due to the stars alone. The equation of mass continuity is, again to linear order,

$$\frac{\partial \rho_1}{\partial t} + \rho_0\,\nabla\cdot\boldsymbol{u}_1 = 0. \tag{4}$$

In practice, the term $\nabla\Phi_1^*$ in the momentum equation is relatively small. However, this term cannot be discarded, as it is the stellar gravity that ultimately drives the outgoing waves.

The next step is to manipulate equations (3) and (4) to obtain a wave equation for ρ_1. Taking the divergence of equation (3) yields

$$\nabla\cdot\frac{\partial \boldsymbol{u}_1}{\partial t} = -\frac{c_{\rm s}^2}{\rho_0}\,\nabla^2\rho_1 - \nabla^2\Phi_1^*.$$

But the time derivative of equation (4) may be cast as

$$\nabla\cdot\frac{\partial \boldsymbol{u}_1}{\partial t} = -\frac{1}{\rho_0}\,\frac{\partial^2\rho_1}{\partial t^2}.$$

Combining the last two equations yields

$$\nabla^2\rho_1 - \frac{1}{c_{\rm s}^2}\,\frac{\partial^2\rho_1}{\partial t^2} = -\frac{4\pi G\rho_0}{c_{\rm s}^2}\,\rho_1^*, \tag{5}$$

where ρ_1^* obeys Poisson's equation:

$$\nabla^2\Phi_1^* = 4\pi G\rho_1^*. \tag{6}$$

Equation (5) is the inhomogeneous wave equation used in all analyses of dynamical friction in gases. In previous studies, however, the source density ρ_1^* tracks the straight-line trajectory of the

[1] We do not know the physical origin of the velocity dispersion, which may represent magnetically mediated turbulence, as is believed to be the case in local clouds. We follow the conventional route of assuming that this motion is isotropic and contributes an effective pressure acting on the cloud as a whole. In more complete studies of molecular clouds, composite equations of state are employed (e.g. McKee & Holliman 1999). For the present work, a simpler, isothermal equation of state suffices (see also Huff & Stahler 2007).

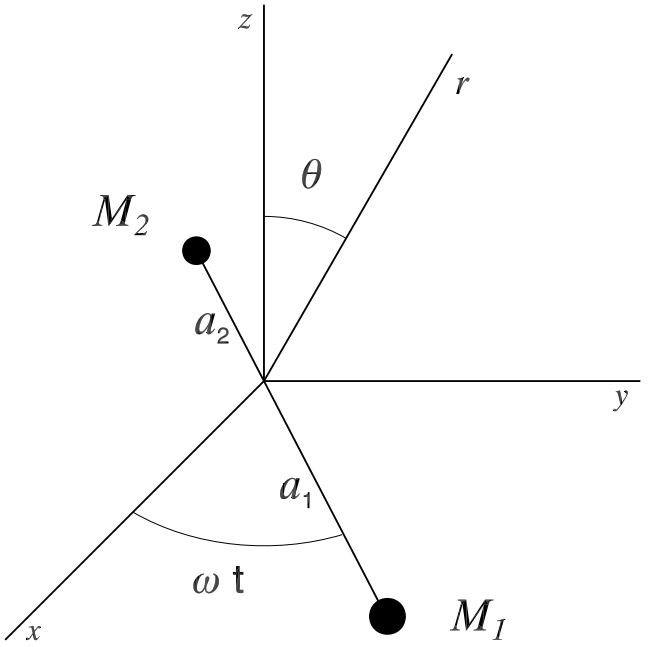

Figure 1. Basic binary parameters. Two stars, M_1 and M_2, orbit their common centre of mass, which is at the origin of the coordinate system. The circular orbits, of radii a_1 and a_2, respectively, lie in the x–y plane. At the time shown, M_1 has swept out the angle $\phi' = \omega t$ from the x-axis.

gravitating mass. After solving the wave equation for ρ_1, the retarding force on that mass is calculated. In our case, the gravitating mass is spatially confined. It is thus more convenient to idealize ρ_1^* as being non-zero only at the origin. This singular, 'equivalent density' for the binary is derived in the next section, where we also show how its temporal change generates acoustic waves.

3 BINARIES AS ACOUSTIC SOURCES

3.1 Potential of the binary

We have written the source term of the wave equation (5) in terms of the equivalent density ρ_1^*. To derive this density, we begin with Φ_1^*, the potential due to the binary. For any spatially compact source, the potential is conveniently expressed as a sum over multipoles. Equation (4.2) of Jackson (1962) gives the electrostatic expression; this is readily altered to the gravitational one:

$$\Phi_1^*(\boldsymbol{x}) \;=\; -4\,\pi\,G \sum_{l=0}^{\infty} \sum_{m=-l}^{l} \frac{q_{lm}}{2l\;+\;1}\;\frac{Y_{lm}(\theta,\phi)}{r^{l+1}}\,. \tag{7}$$

Here, the multipole moments are found from the source density (Jackson 1962, equation 4.3):

$$q_{lm} \;\equiv\; \int Y_{lm}^*(\theta',\phi')\;\left(r'\right)^l\;\rho(\boldsymbol{x}')\,\mathrm{d}^3x'\,. \tag{8}$$

In these two expressions, primed coordinates refer to source points, and unprimed ones to the field points where Φ_1^* is measured.

Fig. 1 shows the binary lying in the x–y plane of our coordinate system, with its centre of mass situated at the origin. Also indicated are two of the three coordinates (r, θ, ϕ) of a field point. At time t, mass M_1 is a distance $r' = a_1$ from the origin and has rotated from the x-axis by the azimuthal angle $\phi' = \omega\,t$, where ω is the binary's angular speed. The other mass M_2 is located at $r' = a_2$ and $\phi' = \omega\,t + \pi$. Both masses have polar angles $\theta' = \pi/2$.

Evaluating the q_{lm} from equation (8), we find that the monopole ($l = 0$) term is

$$\begin{aligned} q_{00} \;&=\; Y_{00}^*\left(\frac{\pi}{2},\omega t\right)\;M_1\;+\;Y_{00}^*\left(\frac{\pi}{2},\omega t+\pi\right)\;M_2 \\ &=\; \frac{M_{\mathrm{tot}}}{\sqrt{4\pi}}\,. \end{aligned} \tag{9}$$

In contrast, all dipole ($l = 1$) terms vanish. For example,

$$\begin{aligned} q_{11} \;&=\; -\sqrt{\frac{3}{8\pi}}\;(a_1 M_1\;-\;a_2 M_2)\;\exp\left(-\mathrm{i}\omega t\right) \\ &=\; 0\,, \end{aligned} \tag{10}$$

by definition of the centre of mass.

The quadrupole ($l = 2$) terms are the most interesting for our purpose. For $m = 0$, we have

$$q_{20} \;=\; -\frac{1}{2}\sqrt{\frac{5}{4\pi}}\,I\,, \tag{11}$$

where $I \equiv M_1\,a_1^2 + M_2\,a_2^2$ is the binary's moment of inertia about its axis of rotation. For $m = 1$,

$$q_{21} \;=\; 0\,, \tag{12}$$

while for $m = 2$,

$$q_{22} \;=\; \frac{1}{4}\sqrt{\frac{15}{2\pi}}\,I\exp\left(-2\mathrm{i}\omega t\right). \tag{13}$$

To complete the set, equation (4.9) of Jackson (1962) tells us that

$$\begin{aligned} q_{2,-1} \;&=\; -q_{21}^* \\ &=\; 0\,, \end{aligned} \tag{14}$$

and

$$\begin{aligned} q_{2,-2} \;&=\; q_{22}^* \\ &=\; \frac{1}{4}\sqrt{\frac{15}{2\pi}}\,I\exp\left(+2\mathrm{i}\omega t\right). \end{aligned} \tag{15}$$

Substitution of these coefficients into equation (7) yields the potential through quadrupole order:

$$\begin{aligned} \Phi_1^* = &-\frac{G\,M_{\mathrm{tot}}}{r}\;+\;\frac{G\,I}{2\,r^3}\left(\frac{3}{2}\cos^2\theta\;-\;\frac{1}{2}\right) \\ &-\frac{3\,G\,I}{8\,r^3}\sin^2\theta\;\{\exp\left[+2\mathrm{i}(\omega t\;-\;\phi)\right] \\ &+\;\exp\left[-2\mathrm{i}(\omega t\;-\;\phi)\right]\}\;, \end{aligned}$$

which simplifies to

$$\begin{aligned} \Phi_1^* = &-\frac{G M_{\mathrm{tot}}}{r} \\ &-\frac{G\,I}{2\,r^3}\left[\frac{3}{2}\sin^2\theta\cos 2(\omega t\;-\;\phi)\;-\;\left(\frac{3}{2}\cos^2\theta\;-\;\frac{1}{2}\right)\right]. \end{aligned} \tag{16}$$

Octupole and higher order terms also exist, but they are of smaller magnitude.

3.2 Equivalent density

We now investigate what distribution of matter generates the potential Φ_1^*. This equivalent density ρ_1^* is a simplified representation of the binary that gives rise, through its fluctuating potential, to the same acoustic waves. Direct calculation reveals that $\nabla^2\,\Phi_1^* = 0$ outside the origin. Thus, the equivalent density is confined to $r = 0$. We already know that the monopole term in Φ_1^* is generated by a

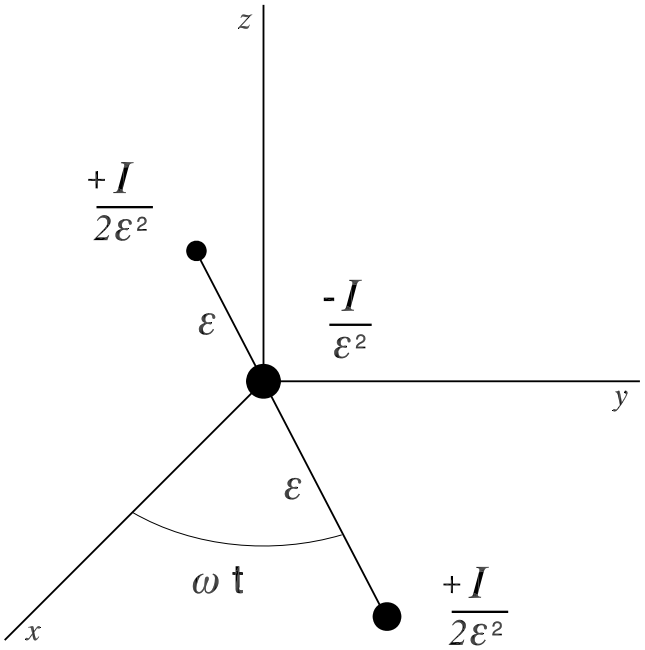

Figure 2. Equivalent system of masses that gives the same gravitational potential, through quadrupolar order, as the actual binary. Two equal masses lie at a distance ϵ on either side of the rotation axis, while a negative mass of twice the magnitude lies at the centre.

mass $M_{\rm tot}$ at the origin. We shall denote this portion of the equivalent density as ρ^*_{10}, and caution the reader not to confuse the double subscript with that in the quadrupole moments q_{lm}. We then have

$$\rho^*_{10} \;=\; M_{\rm tot}\,\delta(x')\,\delta(y')\,\delta(z')\,. \tag{17}$$

Higher multipole terms in the potential similarly have sources, i.e. further contributions to the equivalent density, that are combinations of δ functions and their derivatives, as discussed in Morse & Feshbach (1953, p. 1278).

The quadrupole portion of the equivalent density is illustrated in Fig. 2. Here we show a symmetric placement of point masses that generates the corresponding part of Φ^*_1. We replace the real binary by two equal masses lying along the binary's azimuthal direction within the x–y plane. Each point is at the same small distance ϵ from the z-axis, and the value of each individual mass is $I/2\epsilon^2$. In addition, we place a third point source, with negative mass $-I/\epsilon^2$, at the origin itself.

This configuration clearly has no monopole moment q_{00}, since its total mass vanishes. It may also be verified that all dipole moments are zero. The quadrupole moment for $m = 0$ is

$$\begin{aligned} q_{20} \;&=\; Y^*_{20}\left(\frac{\pi}{2}, \omega t\right)\,\epsilon^2\,\left(\frac{I}{2\,\epsilon^2}\right) \;+\; Y^*_{20}\left(\frac{\pi}{2}, \omega t + \frac{\pi}{2}\right)\,\epsilon^2\,\left(\frac{I}{2\,\epsilon^2}\right) \\ &= -\frac{1}{2}\sqrt{\frac{5}{4\pi}}\,I\,, \end{aligned} \tag{18}$$

in agreement with equation (11). The other quadrupole moments similarly match.

Referring to Fig. 2, the corresponding portion of the equivalent density, which we denote as ρ^*_{12}, is

$$\begin{aligned} \rho^*_{12} \;=\; \frac{I}{2\,\epsilon^2}\,&[\delta(x' - \epsilon\cos\omega t)\,\delta(y' - \epsilon\sin\omega t)\,\delta(z') \\ &+ \delta(x' + \epsilon\cos\omega t)\,\delta(y' + \epsilon\sin\omega t)\,\delta(z') \\ &- 2\,\delta(x')\,\delta(y')\,\delta(z')]\,. \end{aligned} \tag{19}$$

We now expand the arguments of the δ functions to second order in ϵ. For example, we write

$$\delta(x' - \epsilon\cos\omega t) \;=\; \delta(x') \;-\; \epsilon\cos\omega t\,\delta'(x') \;+\; \frac{\epsilon^2}{2}\cos^2\omega t\,\delta''(x')\,.$$

We substitute these series back into equation (19) and multiply them out, retaining only terms through order ϵ^2. Many terms cancel, leaving

$$\rho^*_{12} \;=\; \rho^*_A \;+\; \rho^*_B \;+\; \rho^*_C\,, \tag{20}$$

where

$$\rho^*_A \;\equiv\; \frac{I}{2}\cos^2\omega t\,\delta''(x)\,\delta(y)\,\delta(z) \tag{21a}$$

$$\rho^*_B \;\equiv\; \frac{I}{2}\sin^2\omega t\,\delta(x)\,\delta''(y)\,\delta(z) \tag{21b}$$

$$\rho^*_C \;\equiv\; \frac{I}{2}\sin 2\,\omega t\,\delta'(x)\,\delta'(y)\,\delta(z)\,. \tag{21c}$$

Note that ρ^*_{12} varies temporally with a frequency twice that of the binary itself. The reason for this doubling is that the simplified configuration in Fig. 2 repeats itself every half period. That is, any *difference* in the component masses manifests itself only in higher order multipole terms.

The full equivalent density is

$$\rho^*_1 \;=\; \rho^*_{10} \;+\; \rho^*_{12}\,. \tag{22}$$

Since we have purposefully designed ρ^*_1 to have the same monopole and quadrupole moments as the real binary, the generated potential must be given by equation (16). Nevertheless, an important check is to verify this fact directly, through integration of Poisson's equation. We carry out the relevant calculation in the Appendix.

4 CHARACTER OF THE WAVE

4.1 Prologue: static solution

To find ρ_1, we substitute our expression for ρ^*_1 into the wave equation (5). The static portion of ρ^*_1, given by ρ^*_{10} in equation (17), similarly generates a static contribution to ρ_1, which we denote as ρ^s_1. That is, ρ^s_1 obeys

$$\nabla^2\rho^s_1 \;=\; -\frac{4\,\pi\,G\,\rho_0\,M_{\rm tot}}{c_{\rm s}^2}\,\delta(x)\,\delta(y)\,\delta(z)\,. \tag{23}$$

Because of the linearity of the full wave equation, ρ^s_1 can (and should) be added to the time-varying part we shall derive shortly.

Equation (23) is Poisson's equation, describing the potential from a point mass located at the origin. The value of this fictitious 'mass' is $-\rho_0\,M_{\rm tot}/c_{\rm s}^2$. We may immediately write down the solution:

$$\rho^s_1 \;=\; \frac{\rho_0\,G\,M_{\rm tot}}{c_{\rm s}^2\,r}\,. \tag{24}$$

A similar, but modified, expression applies to the wake created by a moving mass in the traditional dynamical friction problem. Ostriker (1999) has noted that equation (24) is the linear approximation to the full density in a hydrostatic envelope surrounding a gravitating mass $M_{\rm tot}$:

$$\rho(r) \;=\; \rho_0\exp\left(\frac{G\,M_{\rm tot}}{c_{\rm s}^2\,r}\right)\,. \tag{25}$$

The sharp density rise interior to $r = r_{\rm in}$ predicted by equation (25) does not actually occur. As we have described, gas in this region instead goes into free-fall collapse onto the stars.

The linear result given by equation (24) is thus the appropriate form for the static density enhancement.[2] However, ρ_1^s makes no contribution to the angular momentum transport. In calculating the latter, we shall be multiplying the density by the induced, azimuthal velocity. Since the latter oscillates sinusoidally, the product vanishes over a period. We therefore turn to the oscillating density perturbation.

4.2 Wave density

From now on, we may omit ρ_{10}^* when considering the equivalent density. The time-varying density perturbation, which we shall continue to denote simply as ρ_1, obeys

$$\nabla^2 \rho_1 \, - \, \frac{1}{c_{\rm s}^2} \, \frac{\partial^2 \rho_1}{\partial t^2} \, = \, - \frac{4 \pi G \rho_0}{c_{\rm s}^2} \, \rho_{12}^* \, , \tag{26}$$

where ρ_{12}^* is given by equations (20) and (21). We proceed by finding those parts of ρ_1 (denoted as ρ_A, etc.) generated by each additive component of ρ_{12}^*. Linearity of the wave equation ensures that we can add these individual solutions to obtain the full one.

Consider first the functions $\mathcal{D}_A$, $\mathcal{D}_B$ and $\mathcal{D}_C$ obeying

$$\nabla^2 \mathcal{D}_A \, - \, \frac{1}{c_{\rm s}^2} \, \frac{\partial^2 \mathcal{D}_A}{\partial t^2} \, = \, - \frac{2 \, \pi \, G \, \rho_0 \, I}{c_{\rm s}^2} \cos^2 \omega t \, \delta(x) \, \delta(y) \, \delta(z), \tag{27a}$$

$$\nabla^2 \mathcal{D}_B \, - \, \frac{1}{c_{\rm s}^2} \, \frac{\partial^2 \mathcal{D}_B}{\partial t^2} \, = \, - \frac{2 \, \pi \, G \, \rho_0 \, I}{c_{\rm s}^2} \sin^2 \omega t \, \delta(x) \, \delta(y) \, \delta(z), \tag{27b}$$

$$\nabla^2 \mathcal{D}_C \, - \, \frac{1}{c_{\rm s}^2} \, \frac{\partial^2 \mathcal{D}_C}{\partial t^2} \, = \, - \frac{2 \, \pi \, G \, \rho_0 \, I}{c_{\rm s}^2} \sin 2 \, \omega t \, \delta(x) \, \delta(y) \, \delta(z) \, . \tag{27c}$$

If we can find these three functions, then differentiation of their governing wave equations reveals that

$$\rho_A \, = \, \frac{\partial^2 \mathcal{D}_A}{\partial x^2} , \tag{28a}$$

$$\rho_B \, = \, \frac{\partial^2 \mathcal{D}_B}{\partial y^2} , \tag{28b}$$

$$\rho_C \, = \, \frac{\partial^2 \mathcal{D}_C}{\partial x \, \partial y} \, . \tag{28c}$$

Each of the wave equations (27a)–(27c) may be solved using the retarded Greens function. Applying equations (6.54) and (6.66) of Jackson (1962), and integrating over the δ functions, we find

$$\mathcal{D}_A \, = \, \frac{G \, \rho_0 \, I}{2 \, c_{\rm s}^2 \, r} \cos^2 (\omega t \, - \, k r) \tag{29a}$$

$$\mathcal{D}_B \, = \, \frac{G \, \rho_0 \, I}{2 \, c_{\rm s}^2 \, r} \sin^2 (\omega t \, - \, k r) \tag{29b}$$

$$\mathcal{D}_C \, = \, \frac{G \, \rho_0 \, I}{2 \, c_{\rm s}^2 \, r} \sin 2 \, (\omega t \, - \, k r) \, , \tag{29c}$$

where the wave number $k \equiv \omega / c_{\rm s}$.

[2] Actually, equation (24) only gives the static density perturbation to leading order. As we shall see in Section 4.3, another term that dies off as r^{-3} is needed to balance the static part of the quadrupole potential.

In taking spatial derivatives of these last three expressions, we utilize the fact that we are in the far-field limit ($kr \gg 1$). To see this, note first that

$$k^2 \, a_{\rm tot}^2 \, = \, \frac{G \, M_{\rm tot}}{c_{\rm s}^2 \, a_{\rm tot}} \, = \, \frac{2 \, r_{\rm in}}{a_{\rm tot}} \, .$$

Since our field point is located well outside $r_{\rm in}$, we have, for hard binaries,

$$k^2 \, r^2 \, \gg \, k^2 \, r_{\rm in}^2 \, > \, k^2 \, a_{\rm tot}^2 \, .$$

We conclude that

$$k^2 \, r^2 \, \gg \, \frac{2 \, r_{\rm in}}{a_{\rm tot}} \, > \, 1 \, .$$

Following the usual practice in acoustics (e.g. Lighthill 1978), we apply spatial derivatives only to the phase $(\omega t - kr)$. Derivatives of the prefactors of $\mathcal{D}_A$, etc., involving r are smaller by one or two powers of $(kr)^{-1}$.

Differentiation of equations (29a)–(29c), under the far-field approximation, yields expressions for the density components:

$$\rho_A \, = \, - \frac{G \, \rho_0 \, I \, k^2}{c_{\rm s}^2 \, r} \sin^2 \theta \cos^2 \phi \cos 2 \, (\omega t \, - \, k r), \tag{30a}$$

$$\rho_B \, = \, + \frac{G \, \rho_0 \, I \, k^2}{c_{\rm s}^2 \, r} \sin^2 \theta \sin^2 \phi \cos 2 \, (\omega t \, - \, k r), \tag{30b}$$

$$\rho_C \, = \, - \frac{G \, \rho_0 \, I \, k^2}{c_{\rm s}^2 \, r} \sin^2 \theta \sin 2 \phi \sin 2 \, (\omega t \, - \, k r) \, . \tag{30c}$$

Adding these gives the full density perturbation:

$$\rho_1 \, = \, - \frac{G \, \rho_0 \, I \, k^2}{c_{\rm s}^2 \, r} \sin^2 \theta \cos 2 (\omega t \, - \, k r \, - \, \phi) \, . \tag{31}$$

It is important to understand, in a qualitative sense, the amplitude of the density perturbation in equation (31). The relative perturbation, ρ_1 / ρ_0, created by a simple point mass (a monopole) is of the order of $r_{\rm in}/r$, according to equation (24). However, our oscillating density perturbation is quadrupolar. Thus, the monopole result must be multiplied by two powers of $k \, a_{\rm tot}$. The amplitude in equation (31) is indeed of the order of $(r_{\rm in}/r)(k \, a_{\rm tot})^2$.

As expected, the perturbation is an acoustic wave that travels radially outwards with phase velocity $\omega / k = c_{\rm s}$. At any time, the phase of the wave is also dependent on ϕ. In fact, equation (31) reveals that the disturbance may also be viewed as a trailing, two-armed spiral wave, with a latitude-dependent amplitude that peaks at the equator ($\theta = \pi/2$). Since $kr \gg 1$, the spiral is tightly wrapped, with a relatively small pitch angle.

Fig. 3 illustrates the basic geometry of the wave. Shown are wavefronts (surfaces of constant phase) for the two spiral arms in the equatorial plane. If we trace one arm around the circle, the radius of the front increases by $\lambda \equiv 2 \pi / k$. However, because a second arm is interleaved, the actual radial wavelength of the disturbance is $\lambda / 2$, with an associated wavenumber of $2 \, k$. The perturbation's angular frequency is $2 \, \omega$, so the outward velocity is again $2 \omega / 2 k = c_{\rm s}$.

4.3 Induced velocity

We next determine the velocity created in the gas by the passing wave. Taking the curl of the momentum equation (3), we find that

$$\frac{\partial}{\partial t} \, (\nabla \times \boldsymbol{u}_1) \, = \, 0 \, .$$

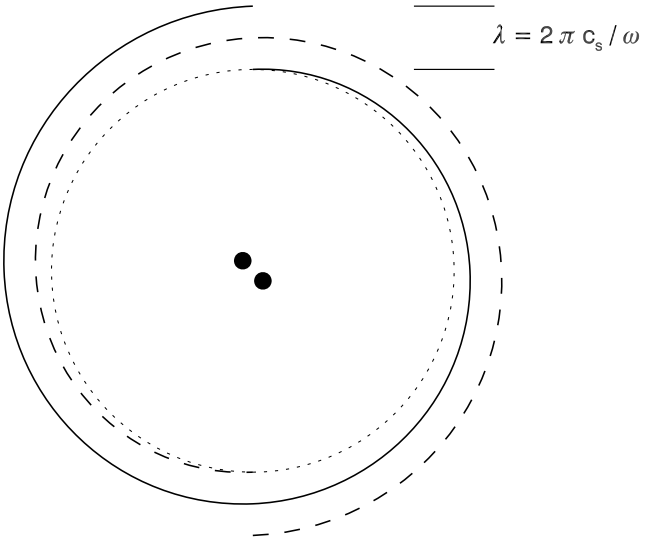

Figure 3. Geometry of the acoustic wave. The radial wavelength of a single spiral arm is λ, as shown. However, because a second arm is interleaved, the actual distance between successive wave crests is λ/2. The central binary is rotating counterclockwise at angular speed ω.

Thus, the induced vorticity is independent of time and is zero for oscillatory motion. It follows that the velocity may be written as

$$\boldsymbol{u}_1 \;=\; \nabla\psi_1\,, \tag{32}$$

where ψ_1 is the velocity potential. From the mass continuity equation (4), ψ_1 obeys

$$\nabla^2\psi_1 \;=\; -\frac{1}{\rho_0}\,\frac{\partial\rho_1}{\partial t}\,. \tag{33}$$

If we assume that ψ_1 depends on the same phase as ρ_1, then the dominant contribution to $\nabla^2\psi_1$ in the far-field limit is simply $-4\,k^2\,\psi_1$. Using $\rho_1(t)$ from equation (31), we find that

$$\psi_1 \;=\; \frac{G\,I\,\omega}{2\,c_{\rm s}^2\,r}\,\sin^2\theta\,\sin 2(\omega t\;-\;kr\;-\;\phi)\,. \tag{34}$$

Finally, we may read off from equation (32) the velocity components

$$u_r \;=\; -\frac{G\,I\,\omega^2}{c_{\rm s}^3\,r}\,\sin^2\theta\,\cos 2(\omega t\;-\;kr\;-\;\phi), \tag{35a}$$

$$u_\theta \;=\; +\frac{G\,I\,\omega}{2\,c_{\rm s}^2\,r^2}\,\sin 2\theta\,\sin 2(\omega t\;-\;kr\;-\;\phi), \tag{35b}$$

$$u_\phi \;=\; -\frac{G\,I\,\omega}{c_{\rm s}^2\,r^2}\,\sin\theta\,\cos 2(\omega t\;-\;kr\;-\;\phi)\,. \tag{35c}$$

In deriving u_r, we again applied the radial derivative to the phase only. We also see that this velocity component is larger than the other two by a factor of the order of $\omega\,r/c_{\rm s} = k\,r \gg 1$. Such dominance of the radial velocity is expected for a wavefront with small pitch angle. While relatively small, the ϕ-component is critical for angular momentum transport.

We may also obtain $\boldsymbol{u}_1$ directly from the momentum equation (3). The gradient of the monopole contribution to Φ_1^* is balanced by the static density perturbation previously derived. Equation (16) shows that there is also a static part of the quadrupolar potential. This is balanced by a smaller term in the static density perturbation. That is, the total static perturbation, to quadrupole order, is

$$\rho_1^s \;=\; \frac{\rho_0\,G\,M_{\rm tot}}{c_{\rm s}^2\,r}\;-\;\frac{\rho_0\,G\,I}{2\,c_{\rm s}^2\,r^3}\,\left(\frac{3}{2}\cos^2\theta\;-\;\frac{1}{2}\right)\,. \tag{36}$$

The remaining, oscillatory part of Φ_1^* contributes in principle to the fluctuating velocity. However, if we actually compare its gradient to the force associated with the pressure gradient, we find the Φ_1^*-gradient to be smaller by several powers of $(k\,r)^{-1}$. In the far-field limit, therefore, the velocity is actually generated only by ρ_1, as equation (33) already indicates. If we express the oscillating part of ρ_1 as the real part of a complex exponential, and set

$$\frac{\partial\boldsymbol{u}_1}{\partial t} \;=\; 2\,i\,\omega\,\boldsymbol{u}_1\,,$$

then we may solve the momentum equation for $\boldsymbol{u}_1$ itself, obtaining the same velocity components as above.

5 ANGULAR MOMENTUM AND ENERGY TRANSPORT

5.1 Braking torque

Imagine surrounding the binary with a spherical shell of radius r. We wish to determine the outflow of angular momentum through this shell. For the acoustic wave to have the properties we ascribed to it, r must lie between $r_{\rm in}$ and $r_{\rm gas}$. The z-component of specific angular momentum at any point on the shell is $r\,\sin\theta\,u_\phi$, with u_ϕ given by equation (35c). Additionally, the mass flux through this same point is $\rho\,u_r$, where u_r is taken from equation (35a). The flux of angular momentum, which we denote as j, is therefore

$$j \;=\; \rho\,r\,\sin\theta\,u_r\,u_\phi \tag{37a}$$

$$\;=\; \frac{\omega^3}{c_{\rm s}^5}\,\frac{\rho_0\,G^2\,I^2}{r^2}\,\sin^4\theta\,\cos^2 2(\omega t\;-\;kr\;-\;\phi)\,. \tag{37b}$$

In the last expression, we have used for ρ its equilibrium value ρ_0. Since the product $r\,\sin\theta\,u_r\,u_\phi$ already falls off as r^{-2}, any density variation that declines with radius does not appear in the total angular momentum efflux, integrated over the sphere.

By angular momentum conservation, this outflow, which we denote $\dot{J}$, must also be $-\Gamma$, where Γ is the torque exerted on the binary by surrounding gas. That is,

$$\Gamma \;=\; -r^2\int_0^\pi {\rm d}\theta\,\sin\theta\int_0^{2\pi}{\rm d}\phi\;j\,. \tag{38}$$

Using

$$\int_0^\pi {\rm d}\theta\,\sin^5\theta\int_0^{2\pi}{\rm d}\phi\,\cos^2 2(\omega t\;-\;kr\;-\;\phi) \;=\; \frac{16\,\pi}{15}\,,$$

we arrive at our main result:

$$\Gamma \;=\; -\frac{16\,\pi}{15}\,\frac{\omega^3}{c_{\rm s}^5}\,\rho_o\,G^2\,I^2\,. \tag{39}$$

A striking aspect of the torque is its high sensitivity to the sound speed $c_{\rm s}$. It is more difficult to gather hotter gas into the wakes that actually provide the gravitational tug on the orbiting stars. An inverse dependence on $c_{\rm s}$ is also present in the expressions for ρ_1 and $\boldsymbol{u}_i$ (see equations 31 and 35a–35c). In any event, the sensitivity of Γ to $c_{\rm s}$ means that quantitative conclusions regarding astrophysical effects of the torque are necessarily rather imprecise.

5.2 Energy loss

The outgoing acoustic wave transports not only angular momentum, but also mechanical energy. We first note, from equations (35a)–(35c) and the succeeding comments, that the kinetic energy density

in the far field simplifies to

$$\frac{1}{2}\,\rho\left(u_r^2 + u_\theta^2 + u_\phi^2\right) \rightarrow \frac{1}{2}\,\rho_0\,u_r^2\,.$$

Now the *total* energy density of any acoustic wave, including the component associated with compression by the enhanced pressure, is twice this kinetic value (Lighthill 1978, section 1.3). Since the wave travels radially outwards at the sound speed, the total energy flux past any point is

$$\dot{\mathcal{E}} = \rho_0\,u_r^2\,c_\mathrm{s}\,. \tag{40}$$

It is instructive to compare this result with j, the angular momentum flux in equation (37a). From equations (35a) and (35c), we have

$$u_\phi = \frac{c_\mathrm{s}}{\omega}\,\frac{u_r}{r\sin\phi}\,.$$

Thus, the angular momentum flux may be written as

$$j = \frac{c_\mathrm{s}}{\omega}\,\rho_0\,u_r^2\,, \tag{41}$$

where we have again replaced the density by its equilibrium value. Integrating $\dot{\mathcal{E}}$ and j over the entire shell, we obtain a relationship between the global energy loss rate $\dot{E}$ and $\dot{J}$:

$$\dot{E} = \omega\,\dot{J}\,. \tag{42}$$

Since both the energy and angular momentum are being extracted from the binary, the same relationship between their loss rates should apply to that system. We now show that this is the case. Referring back to Fig. 1, the angular momentum of the binary is

$$\begin{aligned} J_\mathrm{bin} &= M_1\,a_1^2\,\omega + M_2\,a_2^2\,\omega \\ &= I\,\omega\,. \end{aligned} \tag{43}$$

The binary's total energy is

$$E_\mathrm{bin} = \frac{1}{2}\,I\,\omega^2 - \frac{G\,M_1\,M_2}{a_\mathrm{tot}}\,.$$

But we also have

$$\frac{G\,M_\mathrm{tot}}{a_\mathrm{tot}^3} = \omega^2\,. \tag{44}$$

From this last equation, applying standard manipulations, we find that the potential energy is

$$-\frac{G\,M_1\,M_2}{a_\mathrm{tot}} = -I\,\omega^2\,,$$

so that

$$E_\mathrm{bin} = -\frac{1}{2}\,I\,\omega^2\,. \tag{45}$$

Comparison with equation (43) reveals that

$$E_\mathrm{bin} = -\frac{\omega}{2}\,J_\mathrm{bin}\,. \tag{46}$$

We next relate the temporal change of J_bin to that of ω. We first note that the binary's moment of inertia may be written in terms of the separation a_tot and mass ratio q:

$$I = \frac{q}{(1+q)^2}\,M_\mathrm{tot}\,a_\mathrm{tot}^2\,. \tag{47}$$

Thus, if we again use equation (44) to eliminate a_tot, the angular momentum may be written as

$$J_\mathrm{bin} = \frac{q}{(1+q)^2}\,G^{2/3}\,M_\mathrm{tot}^{5/3}\,\omega^{-1/3}\,. \tag{48}$$

During contraction of the binary, therefore,

$$\frac{\dot{J}_\mathrm{bin}}{J_\mathrm{bin}} = -\frac{1}{3}\,\frac{\dot{\omega}}{\omega}\,. \tag{49}$$

Taking the time derivative of equation (46) and applying equation (49) now give

$$\begin{aligned} \dot{E}_\mathrm{bin} &= -\frac{\dot{\omega}}{2}\,J_\mathrm{bin} - \frac{\omega}{2}\,\dot{J}_\mathrm{bin} \\ &= \frac{3\,\omega}{2}\,\dot{J}_\mathrm{bin} - \frac{\omega}{2}\,\dot{J}_\mathrm{bin} \\ &= \omega\,\dot{J}_\mathrm{bin}\,. \end{aligned} \tag{50}$$

As claimed earlier, the energy and angular momentum of the binary change at the same relative rates as these same quantities in the outgoing wave.

The rate of energy transport by the wave can be recast in another way that provides a check on our derivation. We first note, after applying equation (47) to the negative of equation (39), that

$$\dot{J} = \frac{16\,\pi}{15}\,\frac{q^2}{(1+q)^4}\,\frac{\omega^3}{c_\mathrm{s}^5}\,\rho_0\,(G\,M_\mathrm{tot})^2\,a_\mathrm{tot}^4\,. \tag{51}$$

If we then use equation (44) to eliminate $G\,M_\mathrm{tot}$ in favour of a_tot and ω, we obtain

$$\dot{J} = \frac{16\,\pi}{15}\,\frac{q^2}{(1+q)^4}\,\frac{\omega^7}{c_\mathrm{s}^5}\,\rho_0\,a_\mathrm{tot}^{10}\,.$$

Thus, the energy emission rate can be written as

$$\dot{E} = \frac{16\,\pi}{15}\,\frac{q^2}{(1+q)^4}\,\frac{\omega^8}{c_\mathrm{s}^5}\,\rho_0\,a_\mathrm{tot}^{10}\,. \tag{52}$$

For fixed a_tot, the binary components' relative speed scales with ω. This last expression thus reproduces the fact that the acoustic energy radiated by a quadrupolar source increases as the eighth power of the Mach number (Lighthill 1952).

6 BINARY EVOLUTION

We are now in a position to follow the binary's orbital decay in time. For this purpose, we use for the torque the negative of $\dot{J}$ in equation (51). However, it is now appropriate to eliminate a_tot, again employing equation (44):

$$\Gamma = -\frac{16\,\pi}{15}\,\frac{q^2}{(1+q)^4}\,\frac{\omega^{1/3}}{c_\mathrm{s}^5}\,\rho_0\,(G\,M_\mathrm{tot})^{10/3}\,. \tag{53}$$

We set this torque equal to the temporal derivative of J_bin, as given in equation (48). Rearrangement gives an equation for the evolution of ω:

$$\dot{\omega} = \frac{16\,\pi}{5}\,\frac{q}{(1+q)^2}\left(\frac{G\,M_\mathrm{tot}}{c_\mathrm{s}^3}\right)^{5/3} G\,\rho_0\,\omega^{5/3}\,. \tag{54}$$

Equation (54) is readily integrated. If ω_0 is the initial angular rotation rate, then

$$\omega = \omega_0\left(1 - \frac{t}{t_\mathrm{c}}\right)^{-3/2}\,, \tag{55}$$

where the coalescence time t_c is

$$t_\mathrm{c} \equiv \frac{15}{32\,\pi}\,\frac{(1+q)^2}{q}\,\frac{1}{\rho_0\,G}\left(\frac{G\,M_\mathrm{tot}}{c_\mathrm{s}^3}\right)^{-5/3}\omega_0^{-2/3} \tag{56a}$$

$$\begin{aligned} &= 2\times10^5\ \mathrm{yr}\left(\frac{n}{10^7\ \mathrm{cm^{-3}}}\right)^{-1}\left(\frac{c_\mathrm{s}}{2\ \mathrm{km\ s^{-1}}}\right)^5 \\ &\quad\times\left(\frac{M_\mathrm{tot}}{1\ \mathrm{M_\odot}}\right)^{-5/3}\left(\frac{P_0}{10^3\ \mathrm{yr}}\right)^{2/3}\,. \end{aligned} \tag{56b}$$

At time t_c, ω diverges and the binary has contracted to zero separation. In our numerical evaluation of this time, we have set $q = 1$ and used the initial binary period P_0 in place of the angular velocity ω_0. For $M_{\rm tot} = 1\,{\rm M}_\odot$, a period of 10^3 years corresponds to $a_{\rm tot} = 100\,{\rm au}$.[3]

Finally, we may determine the mechanical energy release of the decaying binary as a function of time. Setting $\dot{E} = -\omega\,\Gamma$ and taking Γ from equation (53), we have

$$\dot{E} = \frac{16\,\pi}{15}\,\frac{q^2}{(1+q)^4}\,\frac{\omega^{4/3}}{c_{\rm s}^5}\,\rho_0\,(G\,M_{\rm tot})^{10/3} \tag{57a}$$

$$= \dot{E}_0\left(1 - \frac{t}{t_{\rm c}}\right)^{-2}. \tag{57b}$$

Here, we have supplied the time dependence of ω from equation (55). The constant $\dot{E}_0$ is

$$\dot{E}_0 \equiv \frac{16\,\pi}{15}\,\frac{q^2}{(1+q)^4}\,\omega_0^{4/3}\left(\frac{G\,M_{\rm tot}}{c_{\rm s}^3}\right)^{10/3}\rho_0\,c_{\rm s}^5\,, \tag{58}$$

and has the value $9 \times 10^{-4}\,{\rm L}_\odot$ for our fiducial parameters. Evidently, the energy release does not rival the radiative loss from the stars themselves until very late during the inspiral, when t is within a few per cent of $t_{\rm c}$. At this point, the stars are separated by several au.

7 DISCUSSION

We may compare, at least in a qualitative manner, our derived torque with that indicated by the traditional theory of dynamical friction. According to equation (12) of Ostriker (1999), the retarding force on a mass M moving at speed V through a cloud of density ρ_0 is

$$F_{\rm DF} = -\frac{4\,\pi\,(G\,M)^2\,\rho_0}{V^2}\,\mathcal{I}\,.$$

The factor $\mathcal{I}$, essentially a Coulomb logarithm, is a non-dimensional function of the Mach number $V/c_{\rm s}$ and the time since the mass first entered the cloud in question. Since $\mathcal{I}$ will generally be of the order of unity, we may ignore it, along with other such factors, in the dimensional argument that follows.

To apply this formula to the binary problem, we interpret V as the components' relative velocity $V_{\rm rel}$, which is $\omega\,a_{\rm tot}$. Then, the torque is of the order of $a_{\rm tot}\,F_{\rm DF}$, so that

$$\Gamma_{\rm DF} \sim -\frac{\omega^3\,\rho_0\,G^2\,I^2}{V_{\rm rel}^5}\,.$$

Here, the moment of inertia has been approximated as $I \approx M\,a_{\rm tot}^2$. Comparison to equation (39) shows that $\Gamma_{\rm DF}$ is the true Γ multiplied by a factor of $(c_{\rm s}/V_{\rm rel})^5$. This factor can be much smaller than unity for the hard binaries of interest. On the other hand, the non-dimensional $\mathcal{I}$ formally diverges for a velocity of $c_{\rm s}$. The traditional theory is thus unreliable in this context.

However, it is not difficult to envision circumstances in which the present theory requires modification. From equation (35a), the Mach number associated with the radial velocity amplitude is

$$\frac{u_r}{c_{\rm s}} = \frac{G\,I\,\omega^2}{c_{\rm s}^4\,r} \tag{59}$$

$$\sim \left(\frac{V_{\rm rel}}{c_{\rm s}}\right)^2\frac{r_{\rm in}}{r}\,. \tag{60}$$

Since $r_{\rm in} \ll r$, the induced velocity is normally subsonic. For binaries that are initially very hard, or late during the inspiral of any system, u_r throughout the far field becomes supersonic. The disturbance then changes character from an acoustic wave to a tightly wound spiral shock. In the same regime, the density perturbation ρ_1 is comparable to or even exceeds ρ_0, so that a fully non-linear treatment is necessary.

Additional modification of the theory would be required by the inclusion of a finite eccentricity in the binary orbits. While the system would still be periodic, the equivalent quadrupolar source would exhibit variation over a continuous distribution of frequencies. The same frequency distribution would then appear in the transmitted waves. It would be interesting to recalculate both the torque and energy loss under this more general condition and thereby follow the evolution of the eccentricity during orbital decay.

Returning to the theory's main astrophysical application, our result for the coalescence time is a reasonable one that adds credence to the underlying picture. The nearest and best-studied region of massive star formation is the Orion Nebula Cluster, whose general population formed 1–2 Myr ago (Hillenbrand 1997). We do not know the age of the high-mass members, the Trapezium, with any precision. Palla & Stahler (2001) have argued that they are relatively young, of the order of 10^5 years, based on the location of BM Ori and its binary companion in the Hertzsprung–Russell diagram. Assuming that the Trapezium stars, along with their companions, are coeval, their inferred age provides an upper bound to the formation time-scale. We are thus encouraged by this matching of times. We stress, however, that our expression for $t_{\rm c}$ in equation (56) varies inversely with the imprecisely known ambient density n.

If massive stars indeed coalesce over such a period, perhaps they do so through an accelerating sequence of binary mergers. The binaries themselves might be created and disrupted rapidly out of the dense gas, leading to a statistically stable period distribution, as originally envisioned by Lynden-Bell (1969). Within this picture, one could in principle determine the mass distribution of the growing population of coalesced objects, thereby advancing the theory another significant step.

ACKNOWLEDGMENTS

This project was originally inspired by extensive discussions with Avery Broderick concerning the formation of massive stars. Kevin Bundy provided useful comments on a preliminary draft of the manuscript. The author was partially supported by NSF grant AST-0908573.

NOTE ADDED IN PROOF

Kim, Kim & Sánchez-Salcedo (2008) have published an alternative solution to this problem. They did not calculate the torque on the binary directly, but rather the radial and azimuthal forces on each star, by numerically integrating over the density ρ_1 derived from equation (5). Their fig. 2 plots these forces as a function of Mach number.

[3]The evolutionary equation (54) neglects accretion from the external medium. A numerical estimate shows that the mass gain is not major for our adopted parameters, but it should be included in a more complete analysis. According to equation (56), any increase of $M_{\rm tot}$ shortens the coalescence time $t_{\rm c}$.

REFERENCES

Bally J., Zinnecker H., 2005, AJ, 129, 2281
Beuther H., Churchwell E. B., McKee C. F., Tan J. C., 2007, in Reipurth B., Jewitt D., Keil K., eds, Protostars and Planets V. Univ. of Arizona Press, Tucson, p. 165
Bonnell I. A., Bate M. R., Zinnecker H., 1998, MNRAS, 298, 93
Butler M. S., Tan J. C., 2009, ApJ, 696, 484
Chandrasekhar S., 1943, ApJ, 97, 255
de Wit W. J., Testi L., Palla F., Zinnecker H., 2005, A&A, 437, 247
Dokuchaev V. P., 1964, Sov. Astron. Astrophys. J., 8, 23
Haisch K. E., Greene T. P., Barsony M., Stahler S. W., 2004, AJ, 127, 1747
Hillenbrand L., 1997, AJ, 113, 1733
Huff E. M., Stahler S. W., 2007, ApJ, 666, 281
Jackson J. D., 1962, Classical Electrodynamics. Wiley, New York
Kim H., Kim W.-T., Sánchez-Salcedo F. J., 2008, ApJ, 679, L33
Kurtz S., Cesaroni R., Churchwell E., Hofner P., Walmsley C. M., 2000, in Mannings V., Boss A. P., Russell S. S., eds, Protostars and Planets IV. Univ. of Arizona Press, Tucson, p. 299
Lighthill J., 1952, Proc. Roy. Soc. A, 211, 564
Lighthill J., 1978, Waves in Fluids. Cambridge Univ. Press, New York
Lynden-Bell D., 1969, in Chrétien M., Deser S., Goldstein J., eds, Astrophysics and General Relativity. Gordon & Breach, New York, p. 1
McKee C. F., Holliman J. H., 1999, ApJ, 522, 313
Morse P. M., Feshbach H., 1953, Methods of Theoretical Physics. McGraw-Hill, New York
Ostriker E., 1999, ApJ, 513, 252
Palla F., Stahler S. W., 2001, ApJ, 553, 299
Rathborne J. M., Jackson J. M., Simon M., 2006, ApJ, 641, 389
Rephaeli Y., Salpeter E. E., 1980, ApJ, 240, 20
Ruderman M. A., Spiegel E. A., 1971, ApJ, 165, 1
Sridharan T. K., Beuther H., Saito M., Wyrowski F., Schilke P., 2005, ApJ, 634, L57
Stahler S. W., Palla F., Ho P. T. P., 2000, in Mannings V., Boss A. P., Russell S. S., eds, Protostars and Planets IV. Univ. of Arizona Press, Tucson, p. 327

APPENDIX A: GRAVITATIONAL POTENTIAL FROM THE EQUIVALENT DENSITY

We wish to verify that ρ_1^* in equation (22) indeed generates the gravitational potential Φ_1^* in equation (16). It is evident that the monopolar portion ρ_{10}^* in equation (17) does yield the term $G\,M_{\rm tot}/r$. We therefore focus on ρ_{12}^*, given in equations (20) and (21), and verify that

$$\Phi_{12}^*(\boldsymbol{x}) \;=\; -G \int \frac{\rho_{12}^*(\boldsymbol{x}')}{|\boldsymbol{x}-\boldsymbol{x}'|}\,{\rm d}^3x'\,, \tag{A1}$$

where

$$\Phi_{12}^* \;\equiv\; -\frac{G\,I}{2\,r^3}\left[\frac{3}{2}\sin^2\theta\cos 2(\omega t\;-\;\phi)\;-\;\left(\frac{3}{2}\cos^2\theta\;-\;\frac{1}{2}\right)\right]\,. \tag{A2}$$

The derivation proceeds in a manner analogous to the calculation of ρ_1 in Section 4.2. We first find three functions $\mathcal{F}_A$, $\mathcal{F}_B$ and $\mathcal{F}_C$ obeying

$$\nabla^2\mathcal{F}_A \;=\; 2\pi G I\cos^2\omega t\;\delta(x)\,\delta(y)\,\delta(z), \tag{A3a}$$

$$\nabla^2\mathcal{F}_B \;=\; 2\pi G I\sin^2\omega t\;\delta(x)\,\delta(y)\,\delta(z), \tag{A3b}$$

$$\nabla^2\mathcal{F}_C \;=\; 2\pi G I\sin 2\,\omega t\;\delta(x)\,\delta(y)\,\delta(z)\,. \tag{A3c}$$

If we further define

$$\Phi_A^* \;\equiv\; \frac{\partial^2\mathcal{F}_A}{\partial x^2} \tag{A4a}$$

$$\Phi_B^* \;\equiv\; \frac{\partial^2\mathcal{F}_B}{\partial y^2} \tag{A4b}$$

$$\Phi_C^* \;\equiv\; \frac{\partial^2\mathcal{F}_C}{\partial x\,\partial y}\,, \tag{A4c}$$

then the combination

$$\Phi_{12}^* \;=\; \Phi_A^* \;+\; \Phi_B^* \;+\; \Phi_C^* \tag{A5}$$

obeys Poisson's equation with ρ_{12}^* as the source density. Equivalently, Φ_{12}^* is the solution of equation (A1).

The functions $\mathcal{F}_A$, $\mathcal{F}_B$ and $\mathcal{F}_C$ are all solutions of Poisson's equation with a central point mass:

$$\mathcal{F}_A \;=\; -\frac{G\,I}{2\,r}\cos^2\omega t \tag{A6a}$$

$$\mathcal{F}_B \;=\; -\frac{G\,I}{2\,r}\sin^2\omega t \tag{A6b}$$

$$\mathcal{F}_C \;=\; -\frac{G\,I}{2\,r}\sin 2\,\omega t\,. \tag{A6c}$$

By successive differentiation of $1/r$, we find

$$\Phi_A^* \;=\; -\frac{G\,I}{2}\left(-\frac{1}{r^3}\;+\;\frac{3x^2}{r^5}\right)\cos^2\omega t \tag{A7a}$$

$$\Phi_B^* \;=\; -\frac{G\,I}{2}\left(-\frac{1}{r^3}\;+\;\frac{3y^2}{r^5}\right)\sin^2\omega t \tag{A7b}$$

$$\Phi_C^* \;=\; -\frac{G\,I}{2}\,\frac{3xy}{r^5}\,\sin 2\,\omega t\,. \tag{A7c}$$

Adding these components yields

$$\begin{aligned}\Phi_{12}^* \;=\; -\frac{G\,I}{2\,r^3}\Big[&\cos^2\omega t\;\left(-1\;+\;3\sin^2\theta\cos^2\phi\right)\\ &+\sin^2\omega t\left(-1+3\sin^2\theta\sin^2\phi\right)\\ &+\sin 2\,\omega t\;\left(3\sin^2\theta\sin\phi\cos\phi\right)\Big]\,,\end{aligned} \tag{A8}$$

which simplifies to equation (A2).

This paper has been typeset from a TEX/LATEX file prepared by the author.